Ernest Henry Halo Exercise

Aims

Understand the inner and outer halo of the Ernest Henry system

- Develop familiarity with available products/data

Understand lateral and vertical zoning patterns

- Mineralogy
- Geochemistry
- Petrophysics

Implications for exploration strategies

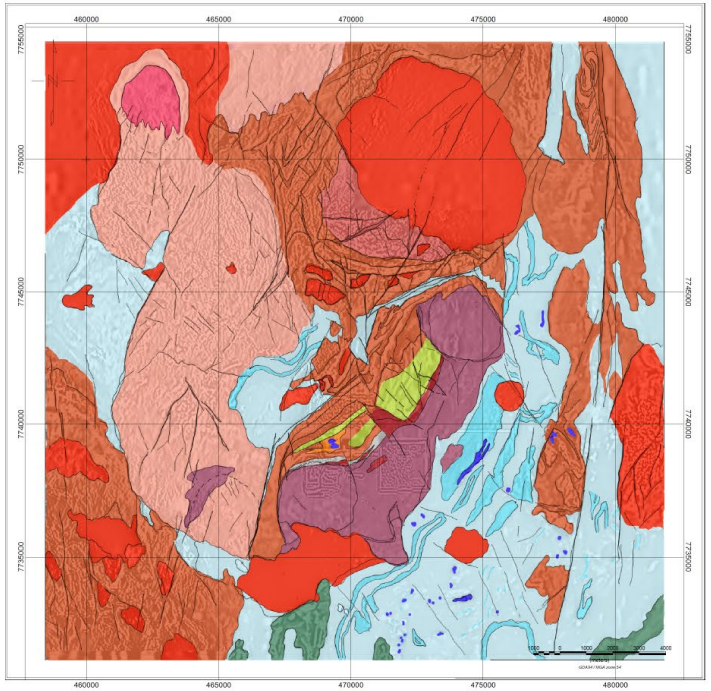

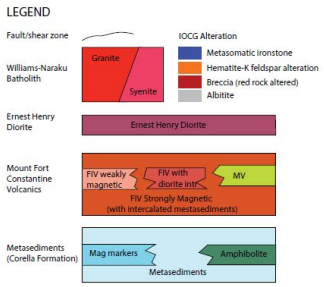

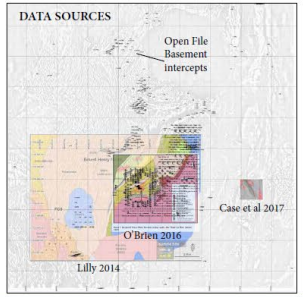

Figure 3.3. (Facing page) Geological interpretation map based on merged open file 50m-spaced aeromagnetic surveys, lithologies from open file drill data, and published maps from the Ernest Henry (Lilly, 2014; O'Brien, 2016) and E1 areas (Case et al, 2017). Map Projection GDA94, MGA54.

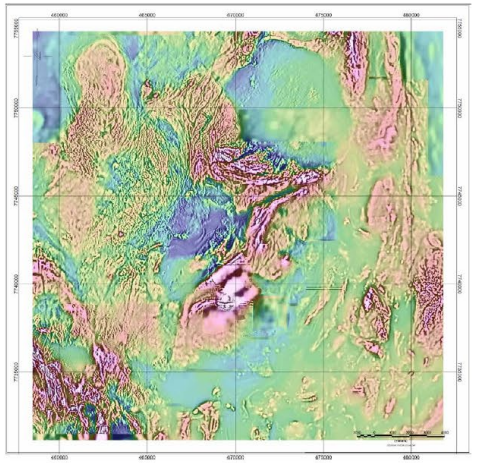

Figure 3.4. Composite aeromagnetic image merging 200m-spaced and 50m-spaced surveys over the area surrounding Ernest Henry - colour Reduced to the Pole magnetics with gaussian stretch overlain on first vertical derivative of RTP. Map Projection GDA94, MGA54.

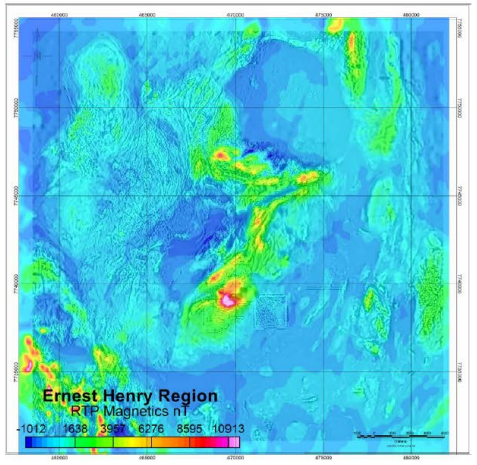

Figure 3.5. Composite aeromagnetic image merging 200m-spaced and 50m-spaced surveys over the area surrounding Ernest Henry - colour Reduced to the Pole magnetics with minimal stretch overlain on first vertical derivative of RTP. Map Projection GDA94, MGA54.

Hydrothermal Alteration	Mineralogy (vein and alteration)	General Alteration Characteristics	Rock Types	Hydrothermal Styles	Spatial relations to Cu-Au mineralisation	Main Chemical Associations
Pre-ore Sodic alteration						
Albitization	albite, titanite, quartz	fine-grained albitization minor titanite, mainly present in altered diorite	diorite, siliciclastic metasedimentary rocks, plagioclase phyric volcanic rocks, calc-silicate rocks	pervasive fine-grained alteration, fracture-controlled breccias, veining	Present over whole area, although lack of preserved alteration in the vicinity of the orebody rare in hanging wall rocks and ore breccia clasts	Na
Na–Ca alteration	actinolite, tremolite, titanite, diopside albite, scapolite, calcite, apatite magnetite, pyrite, quartz	fine-grained albitization minor scapolite and diopside alteration minor titanite, mainly present in altered diorite	diorite, plagioclase phyric volcanic rocks, siliciclastic metasedimentary rocks, calc-silicate rocks	Fracture-related hydrothermal breccia, crackle veining, pervasive alteration	Pervasive throughout term lease, but overprinted by K-feldspar alteration in the vicinity of the ore breccia. Most intense hydrothermal breccias along NE trending fractures	Na, Ca
Magnetite-apatite	magnetite, apatite, actinolite, quartz calcite, quartz	massive fine- to coarse-grained magnetite alteration	plagioclase phyric volcanic rocks	hydrothermal veining, localized pervasive alteration	Present within NE trending fracture systems in the footwall to the deposit	Fe, P, Mg
Potassic alteration						
Biotite–magnetite	biotite, magnetite, K-(Ba) feldspar titanite, quartz	pervasive biotite alteration minor fine-grained K-feldspar with biotite	plagioclase phyric volcanic rocks, siliciclastic metasedimentary rocks	pervasive alteration, rare veining	Pervasive throughout the term lease, and affects all major rock types	K, Rb, Fe, Ba, Mn, Cl
Garnet–K-feldspar–biotite	garnet, biotite, K-feldspar, amphibole quartz, magnetite, pyrite, chalcopyrite	fine- to medium-grained biotite and garnet alteration	plagioclase phyric volcanic rocks, siliciclastic metasedimentary rocks	hydrothermal breccias, localized crackle veining, local pervasive alteration	Present largely in the footwall to the deposit, and occurs up to 1.5 kilometres from the orebody.	Fe, Mn, K, Ba, Cl, Cu, Co
Syn-ore						
K-feldspar	K-(Ba) feldspar, quartz, rutile, calcite	equigranular fine- to medium-grained K-feldspar alteration	plagioclase phyric volcanic rocks, siliciclastic metasedimentary rocks diorite, calc-silicate rocks	pervasive alteration of volcanic rocks, veining	Most intense in the vicinity of the orebody, although occurs as crackle veins up to 2 kilometres from the orebody	K, Rb, Ba, Cl, Cu, Co Ni, As
Sericite	sericite, quartz	pervasive fine- to medium-grained white mica alteration of K-feldspar altered volcanic rocks	plagioclase phyric volcanic rocks	pervasive alteration, localized crackle veining	Overprints K-feldspar altered volcanic rocks, within 400 m of the orebody	K, H
Cu-Au mineralisation						
Breccia	magnetite, pyrite, calcite, biotite, K-(Ba) feldspar,chalcopyrite, barite, molybdenite, arsenopyrite, quartz, electrum, garnet, amphibole, rutile sphalerite, galena, coffinite, monazite	equigranular K-feldspar alteration minor biotite alteration minor garnet and amphibole alteration in calc-silicate rocks minor arsenopyrite and pyrite alteration in siliciclastic metasedimentary rocks	plagioclase phyric volcanic rocks, calc-silicate rocks, siliciclastic metasedimentary rocks	infill-supported hydrothermal breccia, distal crackle veining, distal alteration	Exhibits localization from inner ore breccia to outer crackle veining Elevated Co, As and S up 150 m from ore breccia	Fe, K, Ba, S, Cu, Au, Mn, Ca, C, Sr, Co, As, Mo, Sb, U, Ag, F, Cl
Late veining	K-(Ba) feldspar, magnetite, pyrite, chalcopyrite, fluorite, molybdenite, calcite, garnet, quartz, barite, rutile	no demonstrable alteration	Stage 1 ore breccia	fracture-related veining and breccia	No demonstrable core-margin zonation within ore breccia	Fe, K, Ba, S, Cu, Au, Mn, Ca, C, Sr, Co, As, Mo, Sb, U, Ag, F, Cl

Table 3.1. Summary of Ernest Henry alteration characteristics, from Mark et al (2006)

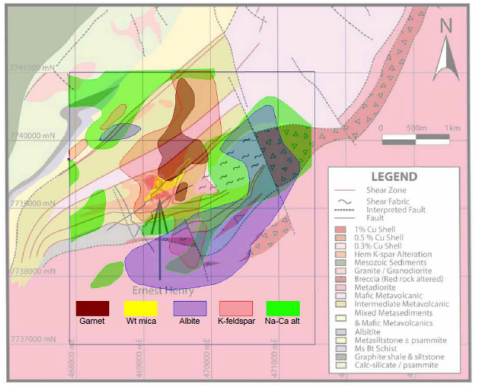

Figure 3.11. Spatial distribution of alteration suites from Mark et al (2006) overlain on the Ernest Henry geological map (O'Brien, 2016). Map Projection AGD84, AMG54.

Figure 3.12. Mineral paragenesis from Mark et al (2006). Line thickness denotes abundance.

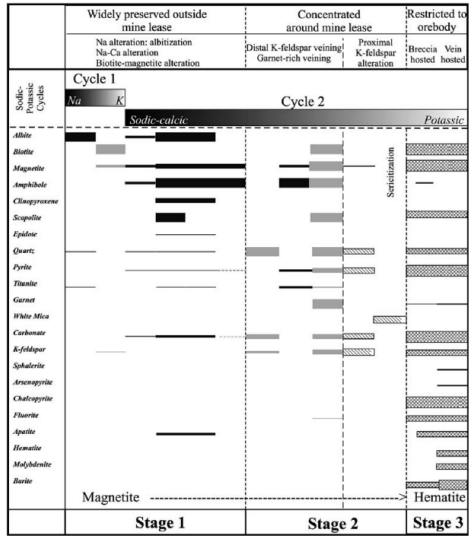

OUTER HALO

Extent

- The widespread cover and regional extent of Na-Ca alteration make it difficult to precisely define the outer halo of the Ernest Henry system. However, the maximum extent of geochemical signatures potentially attributable to Ernest Henry (as opposed to regional Na-Ca alteration) is about 2km to the northeast and approximately 1.5km in all other directions

Geophysical Expression

- Whilst the strongest magnetic anomalies occur in association with the hanging-wall shoot and footwall to Ernest Henry and are not laterally continuous, the zone of elevated magnetic signature continues for approximately 1km to the northeast.
- Mapping of a zone of elevated pyrite extending approximately 1.5km to the north of Ernest Henry and approximately 1km to the south suggests that the halo should be detectable through IP surveying
- While the strongest local gravity anomaly occurs associated with the Ernest Henry ore system, the belt of Mount Fort Constantine Volcanics extending to the northeast also defined a gravity high.
- The 100-150m, 150-200m and 200-300m depth slices of the recently released Isa East airborne EM survey highlight Ernest Henry and the surrounding region as containing conductive sources, though it is unclear whether this response is related in any way to surface infrastructure associated with the mine. The survey aircraft increased altitude to more than 400m over the pit and infrastructure.

Exploration Geochemistry

- Lilly et al (2014) also reported multi-element MMI anomalies in Cu and Mo associated with a zone 4km to the northeast of Ernest Henry, and MMI surveying over the similarly-covered E1 deposit to the southeast of Ernest Henry showed distinct MMI anomalies in Ag, Au, Cu, Co, Mo, Mn and U.

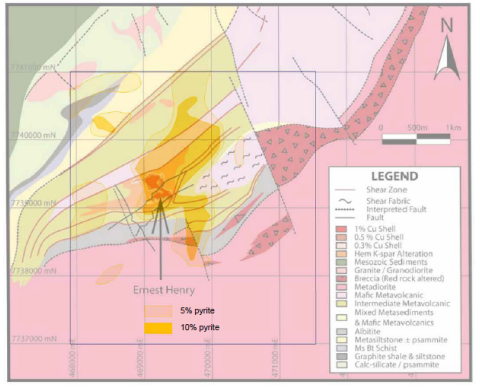

Figure 3.13. Spatial distribution of pyrite percentage from Mark et al (2006) overlain on the Ernest Henry geological map (O'Brien, 2016). Map Projection AGD84, AMG54.

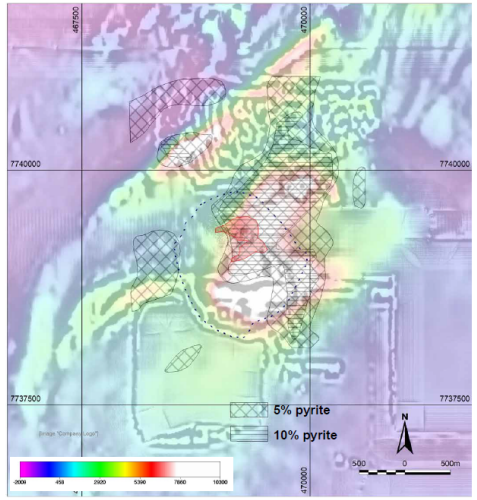

Figure 3.14. Spatial distribution of pyrite percentage from Mark et al (2006) overlain colour RTP magnetics with greyscale VD-automatic gain control image. The zone of abundant pyrite coincides with the orebody itself as well as the magnetite-enriched zone of K-feldspar alteration to the northeast of Ernest Henry, and crosses into the hangingwall on a N-S trend. Map Projection AGD84, AMG54.

Lithogeochemistry

- Analysis of multielement drill data in the Ernest Henry region high lights the following elements as defining a broader outer halo associated with the Ernest Henry system – Bi, Ba, Fe, K and As

Mineralogy

- Consideration of the paragenetic diagram of Mark et al (2006) suggests a number of minerals whose occurrence is diagnostic of the Ernest Henry orebody and halo as opposed to the regional Na-Ca suite. These include fluorite, barite, higher abundances of pyrite, quartz, higher abundances of carbonate, F-rich biotite and Ba-rich K-feldspar.
- Mark et al (2006) compared the composition of biotite and K-feldspar in proximal and distal settings to the orebody, and found that proximal biotites tended to be fluorine-bearing while distal biotites were low in F. In addition, K-feldspars proximal to mineralisation had up to 3% Ba, while more distal K-feldspar showed Ba less than 1%.
- Rusk et al (2010) showed that magnetites associated with Ernest Henry had relatively high Mn/Ti ratios, and that magnetites at Ernest Henry were more Mn-enriched than other hydrothermal magnetite in the region.
- Rusk et al (2010) also reported that apatite at Ernest Henry is unusually hi l fluorine and arsenic compared to other apatites sampled in the region

TIMING OF MINERALIZATION

Relative Timing

Mineralisation is interpreted by Mark et al (2006) to be associated with veining and brecciation which has overprinted the main foliation-forming and metamorphic event. Mineralisation is interpreted to be broadly synchronous with the intrusion of the Naraku batholith.

Absolute age

- Ar-Ar dating of amphibole associated with pre-mineralisation Na-Ca alteration produced ages of approximately 1610Ma (Twyerould, 1997)
- U-Pb dating of titanite associated with pre-mineralisation Na-Ca vein infill produced an age of approximately 1530Ma (Mark et al, 2006), and U-Pb dating of titanite associated with pre-ore bi-mt alteration produced an age of approximately 1514Ma (Mark et al, 2006)
- Ar-Ar dating of biotite and muscovite temporally associated with mineralisation produced ages around 1500Ma (Twyerould, 1997)

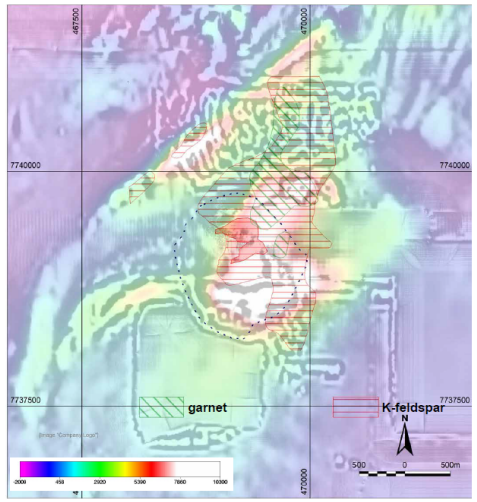

Figure 3.15. Spatial distribution of K-feldspar and garnet from Mark et al (2006) overlain colour RTP magnetics with greyscale VD-automatic gain control image. The zone of K-feldspar coincides with the orebody itself as well as the magnetite-enriched zone to the northeast of Ernest Henry, and crosses into the hangingwall on a N-S trend. Map Projection AGD84, AMG54.

Figure 3.16. Spatial distribution of albite and Na-Ca alteration from Mark et al (2006) overlain colour RTP magnetics with greyscale VD-automatic gain control image. Both zones define a northeast trend coinciding broadly with the strongly magnetic marker in the hangingwall of the Ernst Henry system, broadly defined as the Marshall Shear.. Map Projection AGD84, AMG54.

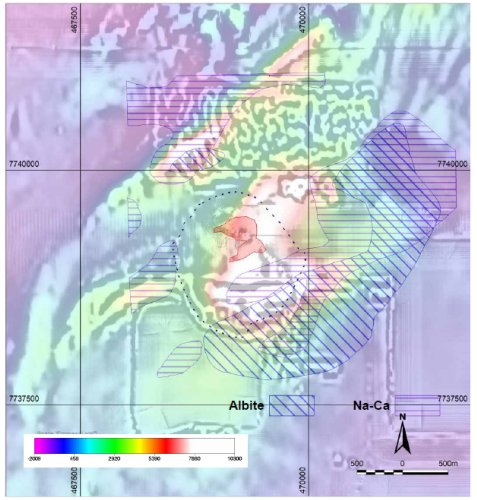

GENETIC MODEL

Ernest Henry is interpreted to be formed as the result of circulation of oxidised, saline, high-temperature Cu-bearing fluids driven by the synchronous intrusion of the Williams-Naraku batholith suite into dilatant zones of competency and redox contrast such as that represented by the footwall, hangingwall and ore sequences at Ernest Henry (eg Oliver et al, 2008; Austin et al, 2017; Murphy et al 2017)

POST-FORMATION MODIFICATION

- Faulting
- Burial by Mesozoic and tertiary sediments
- Surface weathering

EXPLORATION

Discovery Method

The Ernest Henry deposit was discovered on the basis of drilling of a ground TEM anomaly associated the Ernest Henry magnetic anomaly. It was discovered in October 1991 (Lilly et al 2017).

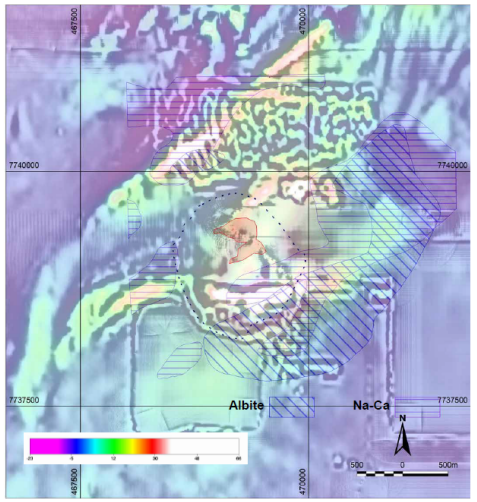

Figure 3.17. Spatial distribution of albite and Na-Ca alteration from Mark et al (2006) overlain colour first vertical derivative magnetics with greyscale VD-automatic gain control image. Both zones define a northeast trend coinciding broadly with the strongly magnetic marker in the hangingwall of the Ernst Henry system, broadly defined as the Marshall Shear.. Map Projection AGD84, AMG54.

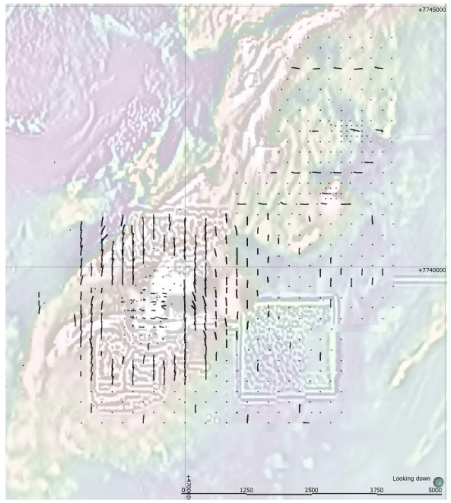

Figure 3.18. Index map showing the distribution of drillholes used in the analysis of lithogeochemical zoning associated with the Ernest Henry area. Map Projection AGD84, AMG54.

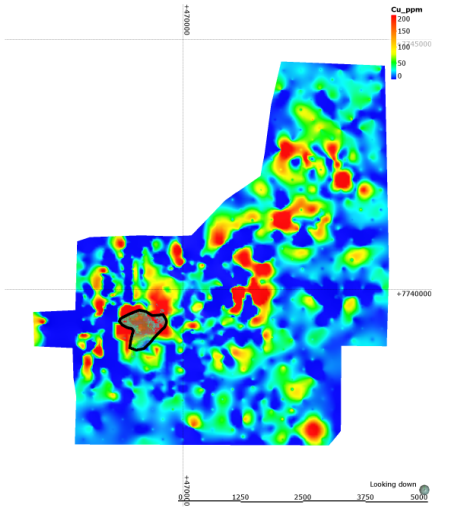

Figure 3.19. Image showing an evaluation of Cu values on the Proterozoic unconformity surface from the multi-element drill dataset. based on a non-directional Leapfrog™ linear interpolant. Solid line denotes the approximate position of the near-surface trace of the Ernest Henry ore outline. Map Projection AGD84, AMG54. Image below shows a 3D perspective view of Cu shells from Austin et al (2017), showing the southerly plunge of the orebody as well as an apparent northerly-dipping intersecting structure down plunge.

Figure 3.20. Image showing an evaluation of Co values on the Proterozoic unconformity surface from the multi-element drill dataset. based on a non-directional Leapfrog™ linear interpolant. Solid line denotes the approximate position of the near-surface trace of the Ernest Henry ore outline. Map Projection AGD84, AMG54. Image below shows a 3D perspective view of Co shells from Austin et al (2017), showing the southerly plunge of the orebody as well as an apparent northerly-dipping intersecting structure down plunge.

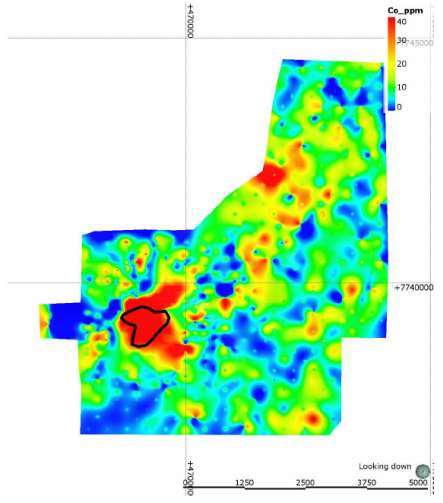

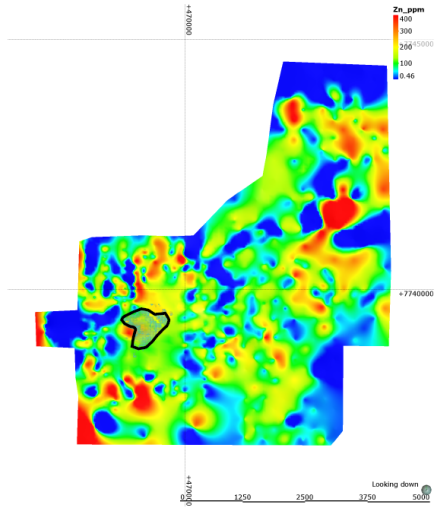

Figure 3.21. Image showing an evaluation of Zn values on the Proterozoic unconformity surface from the multi-element drill dataset. based on a non-directional Leapfrog™ linear interpolant. Solid line denotes the approximate position of the near-surface trace of the Ernest Henry ore outline. Map Projection AGD84, AMG54.

3.2 Element and mineral distributions in drill hole EH691

The distributions of anomalous metals in EH691 are shown in Figure 5 and distributions of major and minor mineral phases determined from TIMA scans are presented in Figure 6 through Figure 8. The mineralogical abundance data was obtained from 49 samples collected at ~12 m intervals over ~560 m of diamond drill core.

The mineralized zone is associated with K-feldspar alteration in contrast to a zone of albite alteration in the hanging wall and andesine alteration in the footwall (Figure 7). The mineralised interval of EH691 (~730 – 950 m) is enriched in Cu-Fe-S ± Co ± Ni ± As. Several distinct zones of Fe, As, Co and Ni enrichment occur across the mineralised zone but the better grades of Ni, S and Co occur between ~730 – 800 m towards hanging wall side of the orebody. Arsenopyrite, cobaltite and gersdorffite were identified in this 730 – 800 m zone (Figure 8). There is a broad negative correlation between S abundance and K-feldspar across the whole mineralised zone. The distribution of pyrite with respect to chalcopyrite reflects the S enrichment, occurring on the upper margins of the mineralized zone at ~720 – 760 m (Figure 6). Muscovite and chamosite also occur in this zone (Figure 7) as does barite, apatite and hornblende (Figure 8).

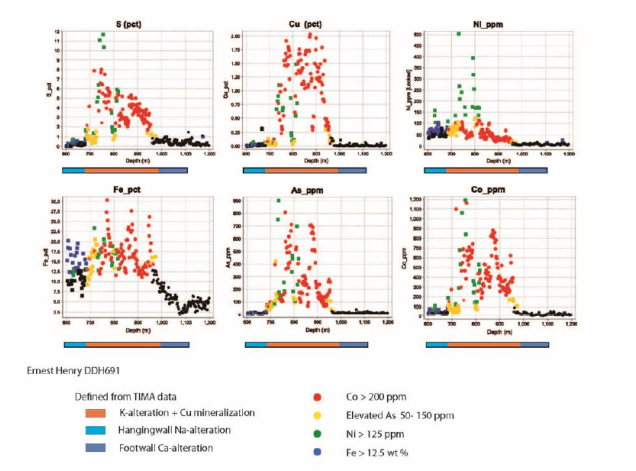

Figure 5: S, Cu, Fe, As, Ni and Co abundances in drill hole EH691 from the EHM dataset.

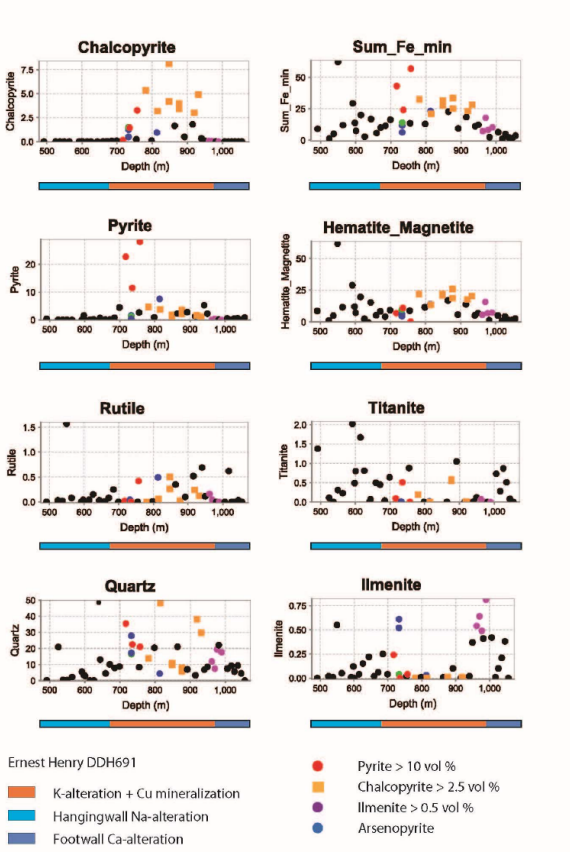

Figure 6: Mineral abundances in drill hole EH691 (vol.%) determined from TIMA scans: chalcopyrite, sum Fe-minerals, pyrite, iron oxide (hematite-magnetite), rutile, titanite, quartz, ilmenite.

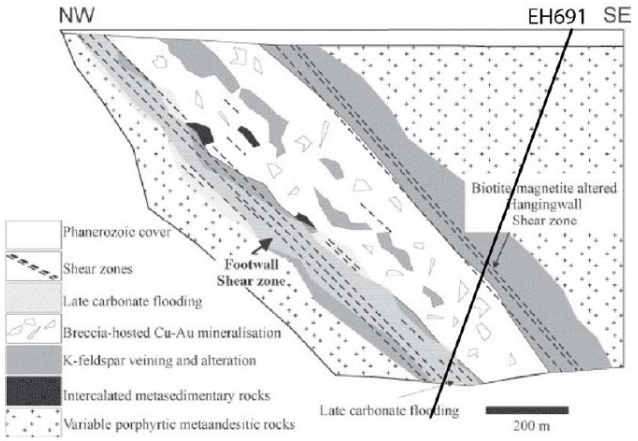

Figure 27: Schematic showing the approximate position of drill hole EH 691 relative to the Ernest Henry ore body, after Mark et al (2005).

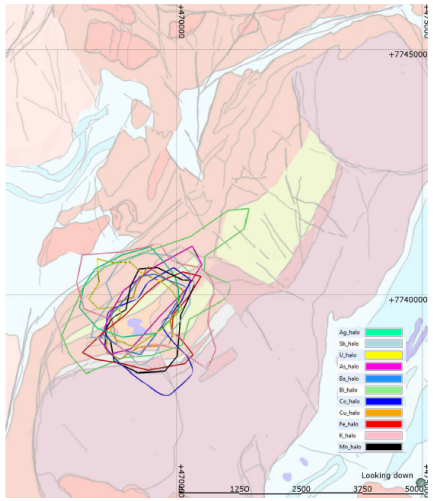

Figure 3.34. Composite outlines showing approximate distribution of elevated values for a range of elements in the Ernest Henry region drill dataset, superimposed on the schematic interpretation map. Map Projection AGD84, AMG54.

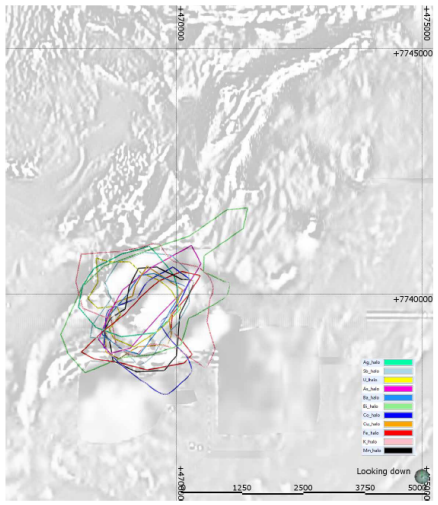

Figure 3.35. Composite outlines showing approximate distribution of elevated values for a range of elements in the Ernest Henry region drill dataset, superimposed on greyscale first vertical derivative. Map Projection AGD84, AMG54.

Figure 3.36. Series of graphs plotting assay values as a function of distance from the 0.5% Cu (eq) shell for the area of strong potassic alteration to the Northeast of Ernest Henry. This area has been singled out as it appears to contain a package of rocks which are most likely to be the lateral equivalent of the Ernest Henry orebody. The box plotted in the diagram below shows the area from which the assay results were obtained in order to make these plots. See text for further discussion.

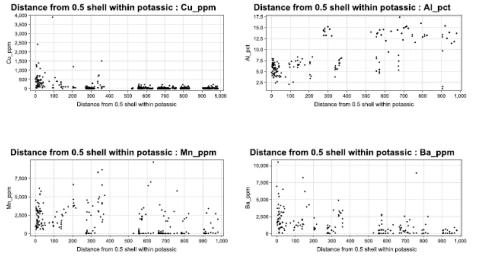

Figure 3.37 (on next pages). Series of element plots on a NE-trending surface clipped to the extent of drilling. Element plots are derived from a non-directional Leapfrog™ linear interpolant of drillhole assay values. Outline shows the outline of the Ernest Henry orebody at a 0.3% Cu equivalent cutoff. The traverse line is interpreted to pass through a zone of K-feldspar-altered metavolcanics which appear likely to be the less-mineralised equivalent of the Ernest Henry host rocks.

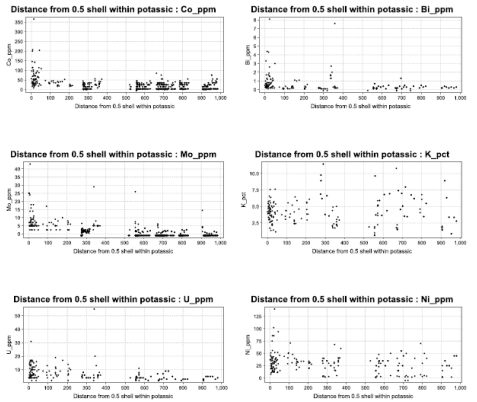

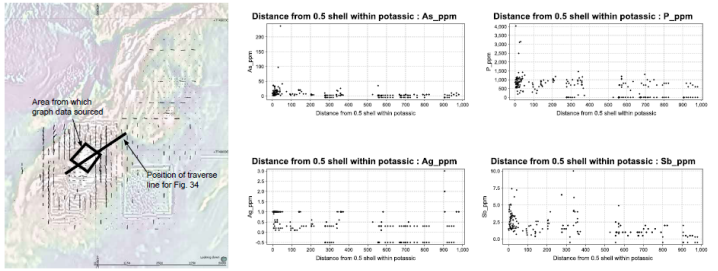

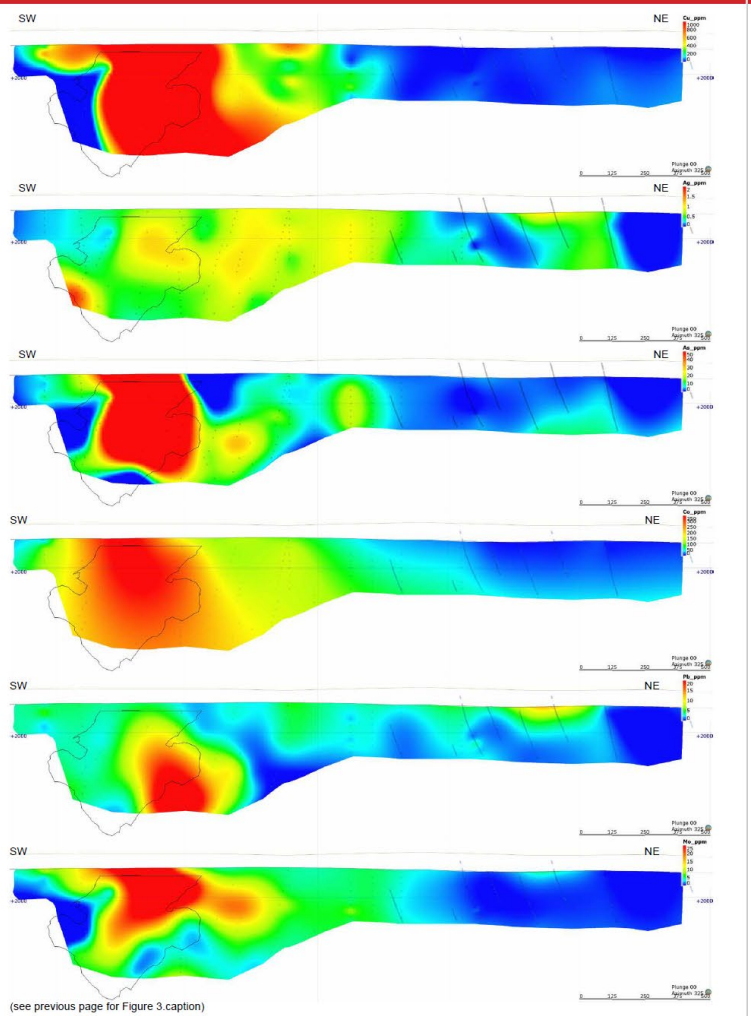

(see previous page for Figure 3.caption)

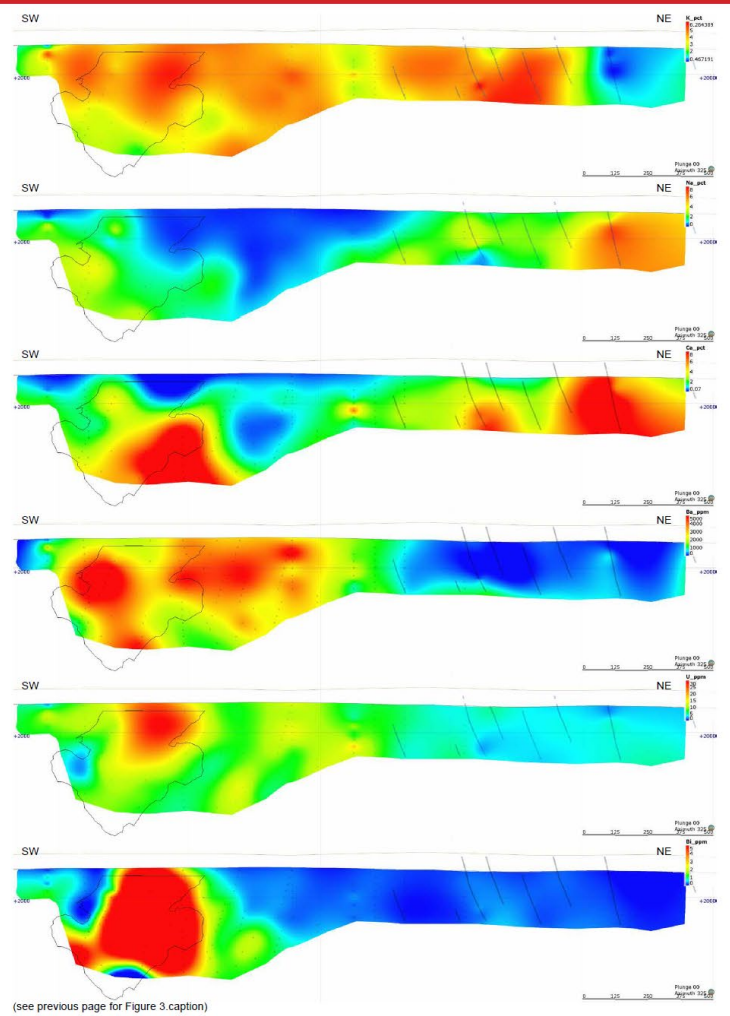

(see previous page for Figure 3.caption)

The other main magnetised zone within the mine area corresponds to the hanging wall shear and in part the breccia body. It has a more subtle magnetic expression due to its lower magnetic susceptibility (~0.5 SI) and more widespread and zoned distribution. In contrast to the highly magnetised discrete zones that coincide with the Marshall and Footwall shear zones, this central part of the anomaly is relatively smooth which reflects both the more rounded shape and diffuse boundaries of the zone and also the magnetic zonation within the body, from ~0.7 – 0.4 SI. There is little by way of petrophysical contrast to isolate the anomaly caused by the hanging wall shear zone from the breccia zone, and hence they are modelled as one here.

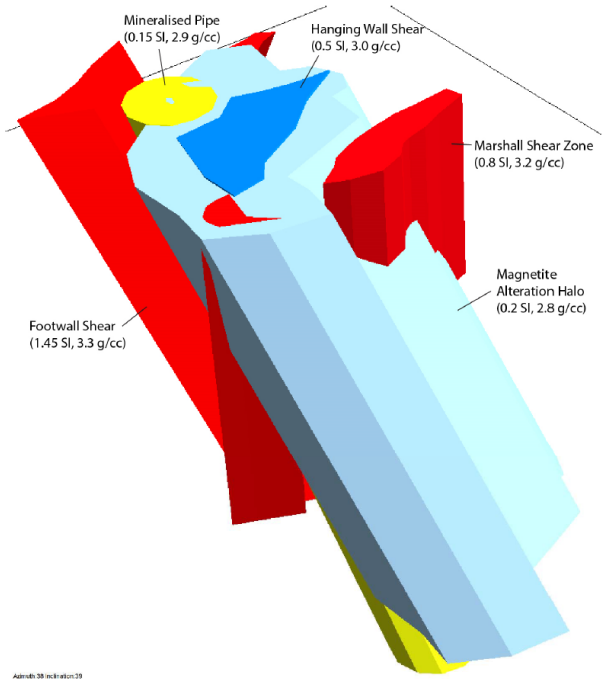

Figure 37: 3-D perspective of the Ernest Henry magnetic model generated in ModelVision™. View is toward the NE.

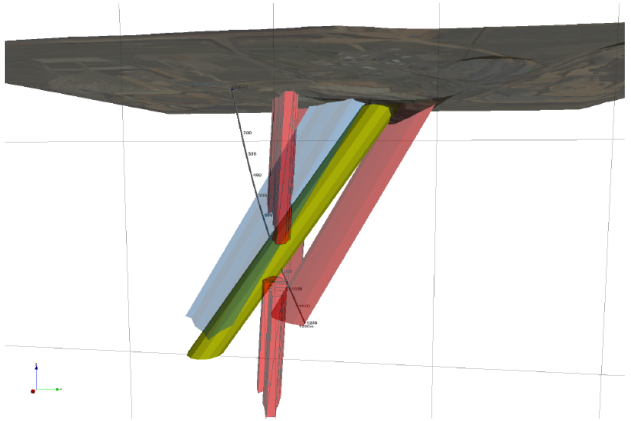

Figure 38: 3-D perspective of the Ernest Henry magnetic model, with the surface topography and drill hole sampled in this project is shown for reference. View is toward the west.

The ore body was modelled by matching the architecture of the pipe, to the Leapfrog™ shells for Cu, Au and Fe. Using this method it was determined that the actual ore-pipe made almost no contribution to the magnetic anomaly, due mainly to its limited spatial extent. However, it is likely that the ore body does have a relatively low susceptibility compared with many of the adjacent rocks, because it is relatively rich in non- or weakly magnetic sulphides, whereas much of the surrounding rock is relatively rich in magnetite. It was necessary to give the mineralised pipe a low susceptibility (<0.15 SI) in order to ensure that it did not create a false anomaly.

Once a model that fits the constraints imposed, and also provides an adequate fit to the magnetic data and the geology was generated, the model was tested against the gravity data. Once reasonable densities, based on measurement in this study, were attributed to the magnetic bodies and the regional (background) gradient was adjusted, a reasonably good match to the gravity data was achieved using bodies from the pre-existing magnetic model.

The main adjustments required were to extend the hanging wall shear/ breccia zone further to the east. This indicates perhaps that this part of the breccia is of comparable density, but with significantly less magnetite. This is consistent with the observation by Keys (2008) that mineralisation and Fe-oxide alteration sit on a west to east gradient across the deposit. Keys (2008) inferred further that the fluids were channelled toward the east, from a source to the west of the deposit (i.e., the NNW-trending). The foot wall shear was also extended both NE and SW, but with much lower susceptibility, and a second sub-parallel magnetised/dense sub-tabular body was added to reflect another shear zone to the north. These relatively simple adjustments were all that was